16TH EUROPEAN CONFERENCE ON EARTHQUAKE ENGINEERING THESSALONIKI 18 - 21 JUNE 2018

EFFECTIVE STIFFNESS AND DRIFT CAPACITY OF MODERN UNREINFORCED MASONRY WALLS

Bastian V. WILDING[1], Katrin BEYER[2]

ABSTRACT

Code design of unreinforced masonry (URM) buildings is based on elastic analysis, which requires as input parameter the effective stiffness and the ultimate drift capacity of the in-plane force-displacement response of URM walls. Eurocode 8, for example, estimates the effective stiffness as 50% of the gross sectional elastic stiffness. Code provisions for the drift capacities are usually empirical equations relating a base drift value to the failure mode and a slenderness ratio. However, comparisons with experimental results have shown that neither approach yields accurate predictions. In this paper, 61 full-scale shear-compression tests of modern URM walls of different masonry typologies from the literature are investigated.

It shows that both the initial and the effective stiffness increase with increasing axial load ratio and that the effective-to-initial stiffness ratios are approximately 75% rather than the used 50%. An empirical model for the computation of the effective-to-initial stiffness ratio is suggested based on a recently developed analytical approach, which attributes the loss in stiffness to diagonal cracking and brick crushing.

As for the drift capacity, the experimental evidence supports the fact that it reduces with increasing axial load and increases with increasing shear span ratio. A recently developed analytical model for the prediction of the ultimate drift capacity for both shear and flexure controlled URM walls is presented. It considers the effect of kinematic and static boundary conditions on the drift capacity. A comparison to test results shows that the proposed models yield better estimates than current code provisions.

Keywords: effective stiffness; drift capacity; unreinforced masonry walls; force-displacement response; shear controlled; flexure controlled

1 INTRODUCTION

In the seismic design of structures two different concepts can be used: force-based and displacement-based design (D'Ayala 2005). In the former, the base shear force for which the structure needs to be designed depends on the mass and the first or several natural frequencies of the structure. To account for the effect of cracking, the dynamic properties of the structures are computed on the basis of effective stiffness rather than gross stiffness values. Furthermore, the global force applied on a system is distributed between the system's load bearing components according to their respective effective stiffnesses.

Displacement-based procedures are mainly used for the assessment of existing structures (Lagomarsino & Cattari 2015; Calvi 1999). Besides strength and stiffness, the deformation capacity of the components is considered too (Fajfar 2000; Priestley et al. 2007). In the case of an unreinforced masonry (URM) wall, the deformation capacity is typically defined as a certain ultimate drift capacity; drift is the horizontal displacement divided by the wall height. The non-linear force-displacement response of said walls, required in displacement-based design, can be approximated by means of a bi-linear curve as shown in Figure 1. Input parameters for the construction of these curves are, among others, the effective stiffness (k_{ef}) and the ultimate drift capacity (δ_{ult}).

[1]PhD-student, EESD, EPFL, Lausanne, Switzerland, bastian.wilding@epfl.ch
[2]Associate Professor, EESD, EPFL, Lausanne, Switzerland, katrin.beyer@epfl.ch

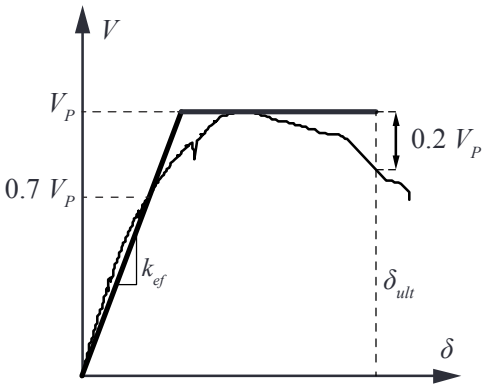

Figure 1. Monotonic shear force-drift response of an URM wall test (Petry & Beyer 2015a) and possible bi-linear approximation with indication of effective stiffness (k_{ef}), peak shear capacity (V_P) and ultimate drift capacity (δ_{ult}), drift is defined as the horizontal displacement by the wall height

Eurocode 8 (EC8) Part 1 (CEN 2004) suggests that the effective stiffness be estimated as half the gross sectional stiffness. In a hyper-static system, approximating the effective stiffness as a fixed percentage of the elastic stiffness means that the forces are effectively distributed proportionally to said stiffness. According to e.g. Salmanpour et al. (2015) and Vanin et al. (2017), the effective stiffness is dependent on the axial load, which is not taken into account by the current EC8 approach.
When determining the effective stiffness from experimental results of shear-compression tests, it is typically defined as the secant stiffness of the wall at 70 % of its peak shear capacity as is also indicated in Figure 1 (Penna et al. 2014; Frumento et al. 2009). For stone masonry walls it is found that in average the effective stiffness corresponds to 50% of their elastic stiffness (Vanin et al. 2017), as proposed by EC8, albeit with a coefficient of variation (CoV) of around 50%.
The ultimate drift capacity of URM walls is often defined as the drift in the post-peak domain at which the shear force drops below 0.8 times the peak shear force (Frumento et al. 2009), see also Figure 1. Many codes contain empirical drift capacity models for URM walls: Eurocode 8 (CEN 2005b), the New Zealand Code (NZSEE 2016), the American standard ASCE 41 (ASCE 2014) and the Swiss Code (SIA 2011). Past studies however have shown that such models lead to a large scatter of the results when compared to tests (Petry & Beyer 2015a). New formulations of empirical drift capacity models can improve the fit (Lang 2002; Petry & Beyer 2014; Salmanpour et al. 2015). Additionally, some drift capacity models are, at least, partly based on mechanical considerations. The analytical approaches by Priestley et al. (2007), Benedetti and Steli (2008) and Petry and Beyer (2015b) are, however, not applicable to shear controlled walls. In Wilding and Beyer (2017a), a mechanics-based model for the drift capacity of both shear and flexure controlled walls is introduced. Yet the model has only been validated so far with a limited data set of wall tests of one masonry typology, i.e. vertically perforated clay brick walls with normal thickness bed-joints and normal strength mortar, and is fairly complex to apply.
The objective of this article is to propose simple formulations for the effective stiffness and the ultimate drift capacity to be used in engineering practice. Experimental evidence from 61 full-scale shear-compression tests of in-plane loaded modern URM walls is presented and parameters that influence the initial and effective stiffness as well as the drift capacity of said walls investigated. Based on test results and existing models (Wilding & Beyer 2017c; Wilding & Beyer 2017b) simple stand-alone equations for the initial stiffness, the effective stiffness and the ultimate drift capacity of in plane loaded URM walls are proposed. The presented formulations are compared to currently used code equations in predicting stiffness and ultimate drift capacity of tests.

2 DATA BASE

The data investigated in the following stems from selected experimental campaigns of full-scale shear-compression tests of modern URM walls. Many of these wall tests have already been used for the calibration of an empirical drift capacity model (Petry & Beyer 2014). Furthermore all of the considered tests have been analysed in Wilding and Beyer (2017b) and Wilding and Beyer (2017c). The following masonry typologies are considered: walls made with clay, calcium silicate and aerated concrete units

and both thin and normal-thickness bed-joints. The selection criteria are: (i) wall height ≥ 1.5 m, wall length ≥ 1.0 m; (ii) constant shear span during test; (iii) constant axial load during test, (iv) availability of the force-displacement history, and (vi) observed brick cracking/crushing.
Only masonry typologies that show brick crushing or at least cracking of the bricks are considered for two reasons. First, the model for the ultimate drift capacity as presented in Sect. 4.2 builds on a plastic hinge model explicitly considering a crushed zone at the wall toe and second, crushing is usually a mechanism that reduces in-plane drift capacities. If no crushing takes place, the drift capacities may be significantly larger due to the development of a sliding plane in the bed-joints. In total, the considered wall tests stem from seven test campaigns (Ganz & Thürlimann 1984; Bosiljkov et al. 2004; Bosiljkov et al. 2006; Magenes et al. 2008; Ötes & Löring 2006; Petry & Beyer 2015a; Salmanpour et al. 2015) and comprise 61 specimens. The present masonry typologies are summarised in Table 1 and an overview of the data is provided in Table 2.

Table 1. Masonry typologies

No.	Typology	No. of walls
1	Vertically perforated clay units with normal thickness bed-joints	41
2	Vertically perforated clay units with thin bed-joints	2
3	Solid calcium-silicate units with normal thickness bed-joints	2
4	Solid calcium-silicate units with thin bed-joints	12
5	Solid aerated concrete units (thin and normal bed-joints)	4

Table 2. Considered experimental campaigns

No.	Reference	No. of walls
1	Petry and Beyer (2015a)	5
2	Bosiljkov et al. (2006)	6
3	Ganz and Thürlimann (1984)	2
4	Salmanpour et al. (2015)	9
5	Bosiljkov et al. (2004)	14
6	Magenes et al. (2008)	15
7	Ötes and Löring (2006)	10

Figure 2 presents the test data by plotting the shear span ratio vs the axial load ratio. As visible, the considered data set covers a rather wide range of shear span and axial load ratios. It shows furthermore that the shear span ratio and the axial load ratio are rather good predictors of the failure mode; the higher the shear span ratio and the lower the axial load ratio, the more likely it is that the wall fails in flexure rather than in shear (Wilding & Beyer 2017c).

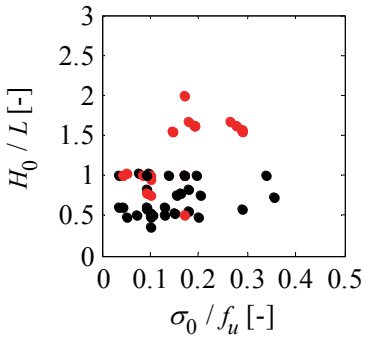

Figure 2. Shear span ratio vs axial load ratio (red: flexure controlled, black: shear controlled)

However, there appears to be a domain in which both modes of failure may occur; this applies to shear span ratios of approximately one with a low to moderate axial load ratio (Wilding & Beyer 2017c). In the following the dataset is analysed for trends in initial and effective stiffness.

3 STIFFNESS

3.1 *Initial stiffness*

3.1.1 *Experimental evidence*

The initial stiffnesses of the considered wall tests are used to back-calculate the elastic modulus per wall test using Timoshenko beam theory [Equation (1)] assuming that the shear modulus is one fourth of the elastic modulus of masonry ($G = ¼\ E$) as suggested in Petry and Beyer (2015b). This value is assumed since there appears to be scientific evidence that the current code estimate of $G/E = 0.4$ (CEN 2005a; ASCE 2014; TMS 2008) is too high for structural elements in masonry (Tomaževič 2009). The G/E ratio is further discussed in Sect. 3.2.

$$E_{init} = k_{init}\left[\frac{H^2\left(H_0 - \frac{H}{3}\right)}{2I} + \frac{4\kappa H}{A}\right] \tag{1}$$

Where H is the wall height, H_0 the shear span, I the gross sectional moment of inertia, κ the shear coefficient and A the gross sectional area. Figure 3a shows the ratio of the back-calculated elastic modulus E_{init} to the masonry compressive strength f_u vs the axial load ratio. There appears to be a general upward trend for the elastic modulus with increasing axial load, which is in line with observations in Vanin et al. (2017) for historical stone masonry walls. Derakhshan et al. (2013) even report an increase in out-of-plane stiffness of URM walls subjected to one-way bending with increasing axial load.

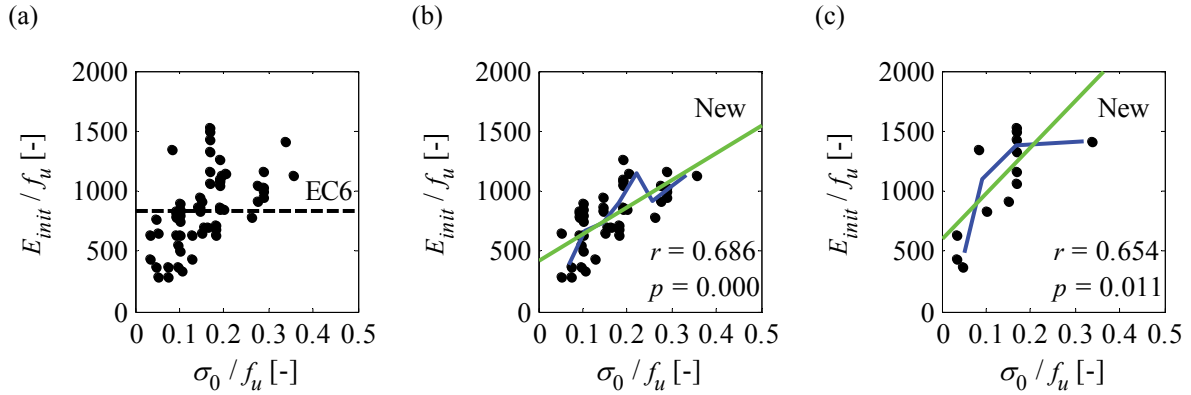

Figure 3. Elastic moduli back-calculated from test results (a) all walls (b) clay brick walls, (c) calcium silicate brick walls; vs axial load ratio

Yet many codes estimate the E-modulus simply as a multiple of the compressive masonry strength f_u. Eurocode 6 (EC6) Part 1 (CEN 2005a), for example, suggests $E = 1000\ f_{u,k}$. Since this paper works with values on the mean statistical level whereas the provision according to EC6 applies to the characteristic one, the EC6 provision is reformulated. EN 1052-1 (CEN 2002) proposes the mean strength to be 20% larger than the characteristic one, which leads to $E = 833\ f_u$. The modified relation is included in Figure 3a as dashed line. It appears not to be in line with the observed trend and may lead to errors when estimating the initial and effective stiffness.

3.1.2 *Proposed model*

Considering the experimental results, two linear regression corves for the elastic modulus based on the axial load may be proposed for practical applications, see Figure 3b, c. It is distinguished between walls with clay bricks and calcium-silicate bricks. Besides the raw data, a moving average (blue line), a linear regression curve of the data (green line), the Pearson correlation coefficient (r) and the p-value (p) are provided. The correlation coefficient is a measure of how well the data corresponds to the linear regression curve; so the higher r, the better the linear correlation represents the actual data. The p-value is a measure of the strength of the evidence against a null hypothesis; the smaller the p-value, the stronger the evidence against said null hypothesis (Sterne 2001). The null hypothesis is: there is *no* correlation between the chosen indicators. A commonly used significance level is $p < 0.05$ (Sterne 2001). For both

types of bricks, the *p*-value suggests that there is a correlation between the ratio of E / f_u and the axial load ratio σ_0 / f_u. The linear regression curves can be approximated as (σ_0 is the axial load on the wall, f_u the masonry compressive strength):

$$E(\sigma_0) = \alpha\, f_u \left(1 + \beta \frac{\sigma_0}{f_u}\right) \tag{2}$$

Where α = 470 for clay brick and α = 720 for calcium silicate brick masonry walls while β = 4 for both types (Wilding & Beyer 2017c).

3.1.3 *Comparison to codes*

In Figure 4a the proposed formulation [Equation (2)] is compared to approaches in EC6 (CEN 2005a) and TMS 402 (TMS 2008) in predicting the elastic modulus of the database of shear-compression tests. EC6 provides an estimate of the elastic modulus, as already mentioned, of $E = 833\, f_u$. The masonry elastic modulus according to TMS 402 is specified as $E = 700\, f_u$ for clay masonry and $E = 900\, f_u$ for concrete masonry. For Equation (2) ('New'), the initial elastic moduli of the wall tests are back-calculated from the measured initial stiffness using a *G*/*E* ratio of 0.25 while for the EC6-approach and the provision according to TMS 402 they are back-calculated using a *G*/*E* ratio of 0.4 as suggested by the respective codes in order to remain consistent throughout the whole prediction process. Both code formulations over-estimate the initial elastic modulus while the proposed approach shows a good median fit and a lower dispersion.

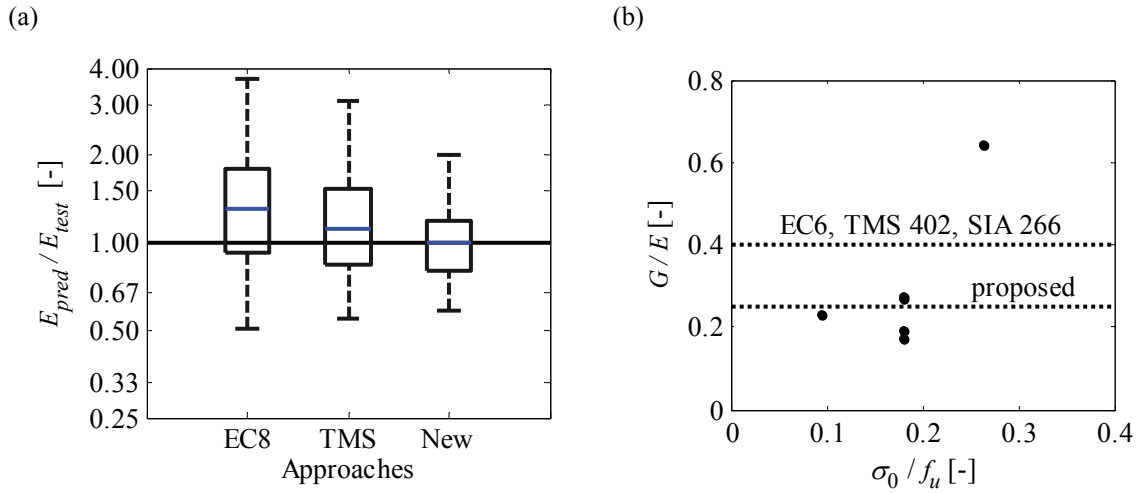

Figure 4. (a) Boxplot of comparison of approaches to predict initial elastic modulus, (b) *G* to *E* ratios back-calculated from test results (Petry & Beyer 2015a) vs axial load ratio

3.2 ***Ratio of shear and elastic modulus***

Many codes (CEN 2005a; TMS 2008; SIA 2015; NZSEE 2016) propose a ratio of shear to elastic modulus of 0.4. According to TMS 402, however, this is not based on any scientific evidence but rather on historic convenience. The ratio has already been put in to question by e.g. Tomaževič (2009), who also suggests a simple approach for estimating the *G*/*E* ratio (neglecting the dependency of the initial stiffness on the axial load) which is outlined in the following. If the elastic modulus has been determined from masonry compression tests, the shear modulus can be retrieved from shear-compression tests (of walls of the same masonry typology) using the determined elastic modulus and a certain measured initial stiffness of the system to compute the shear modulus using Timoshenko beam theory. Based on a measured initial stiffness *k*, the shear modulus can therefore be estimated with the following relation:

$$G = \frac{k\kappa H}{A\left(1 - \frac{kH^2\left(H_0 - \frac{H}{3}\right)}{2EI}\right)} \tag{3}$$

Following this approach for a limited amount of tests, a *G*/*E* ratio of 0.1 is proposed in Tomaževič (2009). In here, the suggested approach of estimating the shear modulus is applied to walls tested by

Petry and Beyer (2015a). The stiffness k is taken as the measured stiffness of the system between 5 and 20 % of the shear force capacity. Figure 4b presents the results by means of a G/E vs axial load ratio plot. It shows that six of the five considered wall tests lead to a G/E ratio of around 0.25, which seems to confirm the assumption made above to use $G = 0.25\ E$.

3.3 *Effective to initial stiffness ratio*

3.3.1 *Experimental evidence*

An overview of the effective-to-initial stiffness ratio in the dataset is provided in Figure 5a. It distinguishes between flexure and shear controlled walls. Independently of the failure mode, the effective stiffness of nearly all walls lies above the estimate according to EC8 Part 1 (CEN 2004), which suggests the effective stiffness be approximated as 50% of the elastic stiffness (dashed line). The test results suggest however that the effective stiffness corresponds in average to around 70-75% of the initial stiffness.

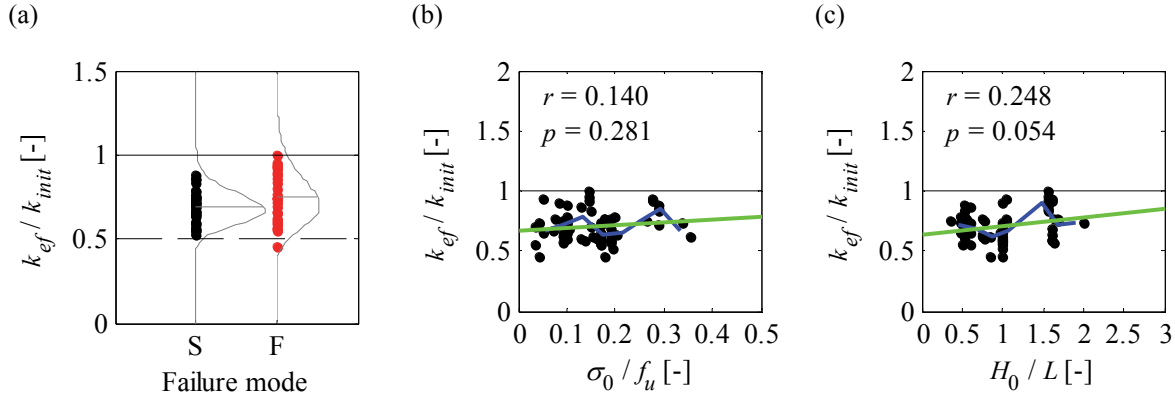

Figure 5. Effective-to-initial stiffness vs (a) failure mode including corresponding lognormal probability distribution functions and indications of mean, (b) axial load ratio, (c) shear span ratio

Furthermore it appears that flexure controlled walls show a slightly larger dispersion around the mean than shear controlled ones. Figure 5a suggests that there is no significant difference concerning the mean value of the effective-to-initial stiffness between the considered masonry typologies. Table 3 sums up the above-mentioned providing the mean and the coefficient of variation (CoV) for the effective-to-initial stiffness ratio per failure mode.

Table 3: Summary of effective-to-elastic stiffness ratio per failure mode

Short	**Indicator**	**mean(k_{ef} / k_{init})**	**CoV(k_{ef} / k_{init})**	**No. wall units**
S	Shear	0.69	0.09	34
F	Flexure	0.75	0.15	27

The effective-to-initial stiffness ratio k_{ef} / k_{init} vs the axial load ratio is presented in Figure 5b. This measure appears to be relatively constant with the axial load ratio, which indicates that also the effective stiffness depends on the applied axial loading. This has already been indicated previously by several authors (Vanin et al. 2017; Salmanpour et al. 2015). Besides the raw data, a moving average (blue line), a linear regression curve of the data (green line), the correlation coefficient (r) and the p-value (p) are provided. Figure 5c plots the same stiffness measure vs the shear span ratio. It appears that there is no significant trend between them.

3.3.2 *Proposed model*

According to the analytical model developed in Wilding and Beyer (2017b) which accounts for the reduction in wall in-plane stiffness due to uplift in bed-joints and diagonal cracking of the wall, the effective stiffness is around 75 % of the initial wall stiffness. This is, furthermore, in agreement with the presented test results. Therefore it is recommended to use 75 % of the initial stiffness as an effective

stiffness estimate:

$$k_{ef} = 0.75\, k_{init} = 0.75\, E_{init} \left[\frac{H^2 \left(H_0 - \frac{H}{3} \right)}{2I} + \frac{4\kappa H}{A} \right]^{-1} \quad (4)$$

In the following section, the relation proposed in Equation (4) is compared to currently used code provisions in predicting the effective stiffness of the tests from the database.

3.3.3 *Comparison to codes and tests*

The considered approaches are briefly re-visited and described before comparing their performance in predicting the effective stiffness of the wall tests from the database. In EC8 Part 1 (CEN 2004) it is suggested that, *in absence of an accurate evaluation of the stiffness properties*, 50 % of the gross sectional elastic stiffness be taken as the effective stiffness. The elastic modulus follows $E = 833\, f_u$ while the shear modulus is obtained taking 40 % of E. ASCE 41 (ASCE 2014) simply states that flexural and shear deformations shall be considered, with an elastic modulus as specified by TMS 402 (TMS 2008): $E = 700\, f_u$ for clay and $900\, f_u$ for concrete masonry respectively. $G = 0.4\, E$. No mention is made about effective or cracked stiffness of the wall. Therefore, the provided un-cracked (initial) stiffness is used for comparison below. In the New Zealand code (NZSEE 2016), the already cracked (effective) elastic modulus is determined as a multiple of the mean compressive strength, $E = 300\, f_u$, while the shear modulus is suggested to follow $G = 0.40\, E$. According to the Swiss code (SIA 2011; SIA 2015; SIA 2014), the characteristic elastic and shear modulus, obtained as in EC8, should be reduced by 70 % in order to obtain the effective (cracked) stiffness of the wall. Concerning the formulation presented in this paper [Equation (4)], the elastic modulus is obtained using Equation (2) while assuming $G/E = 0.25$.

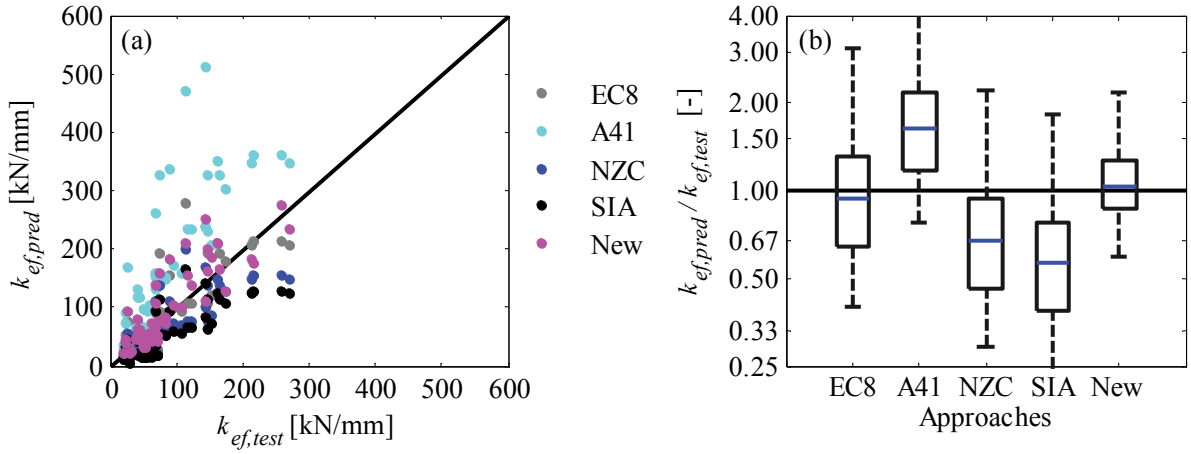

Figure 6. Comparison with code approaches in predicting the effective stiffness of wall tests, (a) predicted vs measured effective stiffness, (b) boxplot

Figure 6 illustrates the performance of the considered approaches in predicting the effective stiffness of the wall tests. Both the presented approach ('New') and the EC8-formulation show a good median fit, the provision according to EC8, however, with a larger deviation. The New Zealand (NZC) and the Swiss code (SIA) significantly underestimate the median effective stiffness, while the American code (A41) overestimates it fairly strongly. Concerning the EC8-provision, it may be worthy adding that despite the good median fit of the provision concerning the effective stiffness, the approach is based on three assumptions that appear not to be entirely correct for the investigated masonry typologies. First, the proposed G/E ratio of 0.4 appears to be too high for masonry walls as already stated by Tomaževič (2009) and indicated further in Figure 4b. Second, the formulation for the initial elastic modulus based on the multiple of the masonry compressive strength ($E_{init} = 833\, f_u$), along with the G/E ratio of 0.4, leads to an initial stiffness that is too high, Figure 4a. Finally, the provision of taking half of the initial stiffness to estimate the effective (cracked) one appears to be too low as the initial-to-effective stiffness ratio seems rather to be found around 0.75, Figure 5a. However, the assumptions' deficiencies seem to cancel each other out when estimating the effective stiffness—too high an initial stiffness is reduced by a factor that is too low—leading to a rather good median fit in predicting the above-mentioned test

results.

4 ULTIMATE DRIFT

4.1 *Experimental evidence*

The database of shear-compression tests as introduced in Sect. 2 is analysed for trends in drift capacity below. Figure 7a presents the reported ultimate drift capacities normalized by the shear span ratio (shear span-to-wall length ratio) including corresponding lognormal distributions vs the observed failure mode. The corresponding statistics can be found in Table 4. The median normalized drift capacity for flexure controlled walls lies at 0.54 % which is significantly smaller than the 4/3 0.8% (~1.07 %) as suggested by EC8 (CEN 2005b).

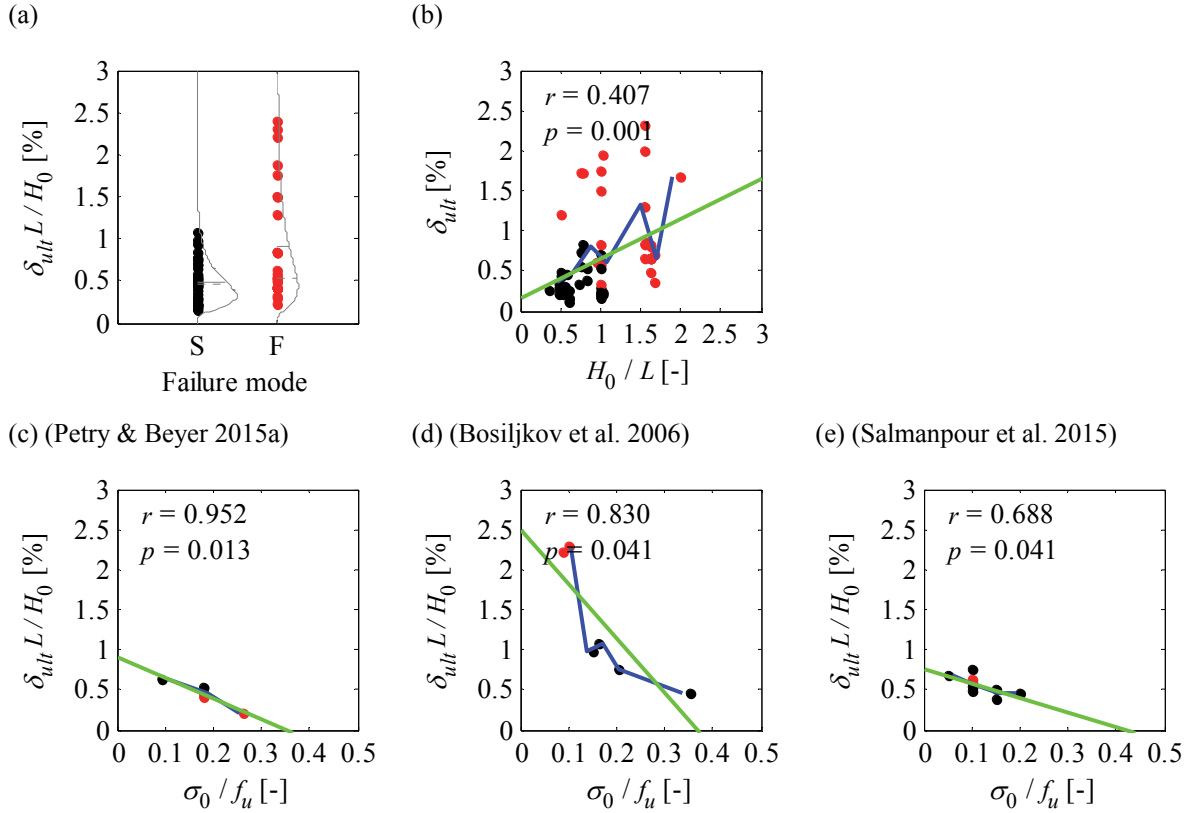

Figure 7. (a) Reported ultimate drifts, normalized by the inverse of the shear span-to-wall height ratio, separated by failure modes including lognormal probability distribution functions, (b) Ultimate drift capacity vs shear span ratio; Normalized ultimate drifts vs axial load ratio per testing campaign; (c) Petry and Beyer (2015a), (d) Bosiljkov et al. (2006), (e) Salmanpour et al. (2015); red: flexure controlled, black: shear controlled walls

Table 4. Summary of statistics for distribution of reported ultimate drift capacities

Short	Indicator	median(δ_{ult} L/H_0)	mean(δ_{ult} L/H_0)	CoV(δ_{ult} L/H_0)	No. wall units
S	Shear	0.47	0.49	0.51	34
F	Flexure	0.54	0.90	0.76	27

Figure 7b shows the ultimate drift capacity vs the shear span ratio, separating the data by observed failure mode. The plot includes the moving average (blue line), a linear regression curve on the data (green line), the correlation coefficient (r) and the p-value (p). There appears to be a fairly clear upward trend for the drift capacity with increasing shear span ratio which has already been observed previously (Petry & Beyer 2014).

The normalized drift capacity vs the axial load ratio is plotted for three testing campaigns additionally distinguishing the failure modes shear and flexure using different markers in Figure 7c, d, e. It can be observed that the three considered campaigns show very clear downward trends for the normalized drift

capacity with increasing axial load ratio for both failure modes. So it may be fair to conclude that there appears to be a downward trend with increasing axial load ratio for both wall types (i.e. shear and flexure controlled) as already stated by various authors (Ganz & Thürlimann 1984; Petry & Beyer 2014; Salmanpour et al. 2015).

4.2 *Proposed model*

Based on the above-mentioned observations, the CDC model (Wilding & Beyer 2017a) and more detailed analysis of the displacement fields of URM shear-compression tests (Wilding & Beyer 2017b), a simple mechanics-based formulation is put forward in Wilding and Beyer (2017c) for the estimation of the ultimate drift capacity.

$$\delta_{ult} = \left(\min\left[\frac{f_{B,c}}{E}; 0.007\right] - \frac{\sigma_0 L}{E l_{cr}}\right)\frac{h_{cr}}{l_{cr}}\left(1 - \frac{h_{cr}}{3H}\right) \quad (5)$$

Where $h_{cr} = h_B\ (0.5 + H_0 / H)$, $l_{cr} = l_B$, L is the wall length, h_B the brick height, l_B the brick length and $f_{B,c}$ the brick compressive strength. Unlike the empirical code provisions, Equation (5) is a mechanics-based equation evaluating a crushed zone at the wall toe with high curvatures at ultimate failure. According to Equation (5), the ultimate drift reduces with increasing axial load and increases with increasing shear span. Both trends are observed in Sect. 4.1. In the next section, current code approaches for estimating the ultimate drift capacity are briefly introduced and, subsequently, compared to Equation (5) by means of predicting the ultimate drift capacities of the walls in the database as introduced in Sect. 2.

4.3 *Comparison to codes and tests*

EC8 Part 3 (CEN 2005b) gives an estimate for the drift at the *Limit State of Near Collapse*, which is considered equivalent to the ultimate drift of the wall. Whichever of the shear force capacity equations yields a smaller value is assumed to determine the behaviour of the wall (shear or flexure controlled) and therefore implicitly the way of prediction of the ultimate drift capacity. The drift capacity for shear controlled walls is set to a constant value (δ_{ult} = 4/3 0.4 [%]) while the one for flexure controlled walls is a base value times the shear span ratio (shear span H_0 by wall length L): δ_{ult} = 4/3 0.8 H_0 / L [%].

The American standard ASCE 41 (ASCE 2014) provides the drift (among other limits) at the *Performance Limit of Life Safety*, which is supposed herein to be approximately equal to the ultimate drift capacity. For bed-joint sliding a constant drift limit of 0.75 % is provided. Yet, for rocking failure, the provision states: δ_{ult} = 100 $u_{tc,r}$ / H with $u_{tc,r}$ being the horizontal displacement *associated with the onset of toe crushing*, which is smaller or equal to a drift of 2.25 %. Furthermore it reads in the commentary section: *The deformation associated with the onset of toe crushing shall* […] *be* […] *established and checked* […] *using a moment-curvature or similar analytical approach.* This appears to indicate that the engineer is free to choose any analytical approach in order to *establish* the required deformation limit $u_{tc,r}$. Another hint is provided in the commentary section of ASCE 41 saying: *The test results indicate* […] *drifts of at least* 1.5 % *are sustainable for certain configurations* […]. In order to consistently compare code provisions without having to resort to models not included in said codes, the drift limit of 1.5 %, as mentioned in the commentary, is used for walls showing a rocking failure.

Dependent on the minimum shear force capacity among the considered failure modes diagonal tensile failure, toe crushing, rocking and bed-joint sliding failure, different *deformation capacities* are provided in (NZSEE 2016). For the first two modes, only the elastic deformation at peak shear force is permitted (i.e. shear force by effective wall stiffness), while for the latter two actual drift limits are provided: min[0.3 H / L; 1.1] [%] for rocking failure and a constant drift of 0.3 % in case of the bed-joint sliding mode leading to the lowest shear force capacity.

According to the Swiss code SIA D 0237 (SIA 2011), the *deformation capacity* of the wall is to be determined taking into account the boundary conditions a wall is subjected to without considering the predicted failure mode. The relation which is based on the work of (Lang 2002) can be given as follows:

$$\delta_{ult} = 0.8\ [\%]\left(1 - \frac{\sigma_0}{f_u}\right)\frac{H_0}{H} \quad (6)$$

Where σ_0 is the axial load on the wall, f_u the masonry compressive strength and H_0 / H the shear span-to-wall height ratio. Figure 8 compares the performance of the presented code approaches and the model introduced in Sect. 4.2 in predicting the results of the database of shear-compression tests. All approaches show a large scatter. The EC8 (CEN 2005b) and ASCE 41 (ASCE 2014) predictions are mainly too high, while the New Zealand code (NZSEE 2016) generally underestimates the ultimate drift capacities. The SIA-formulation (SIA 2011) and the equation proposed in here ('New') show a rather good median fit, both however with a large dispersion.

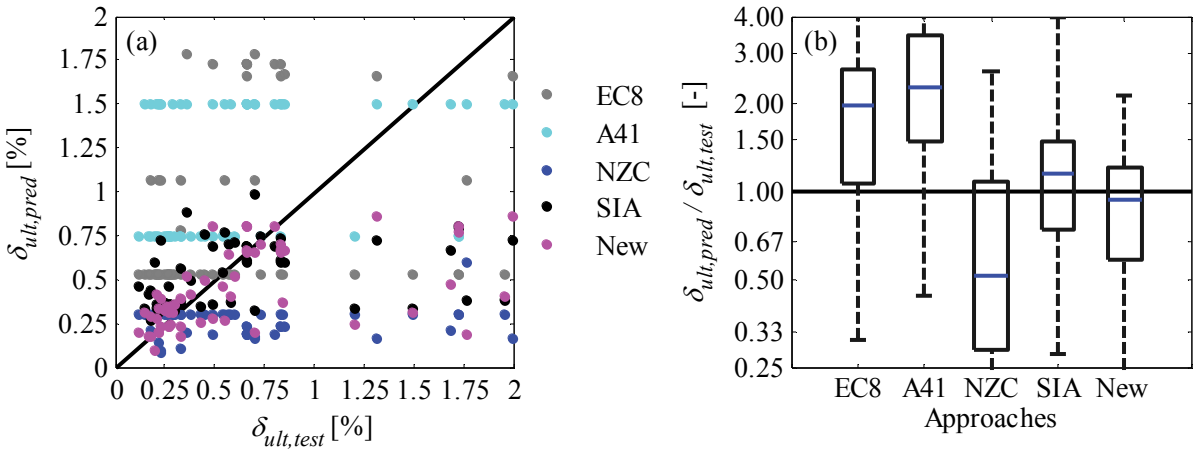

Figure 8. Comparison with code approaches in predicting the ultimate drift capacity of wall tests, (a) predicted vs measured ultimate drift capacity, (b) boxplot

As visible in Figure 8a, tests with drift capacities of more than 1 % are largely underestimated by the considered approaches, which results at least in predictions on the safe side for those cases. Walls with a drift capacity larger than 1 % are typically characterized by a low axial load ratio. If those walls also show a low shear span-to wall height ratio, their behaviour may be governed by bed-joint sliding to reach such high drifts while in the case of a higher shear span-to-wall height ratio their response would be characterized by rocking with limited toe crushing at ultimate failure. Yet these types of walls do usually not govern the force-displacement response of a building as they only carry a small share of the axial load. When neglecting tests with drift capacities larger than 1 %, the fit of the proposed formulation can be significantly improved as is shown in Figure 9, while the EC8, the ASCE 41 and now also the SIA formulations all lead to a significant overestimation of the drift capacities.

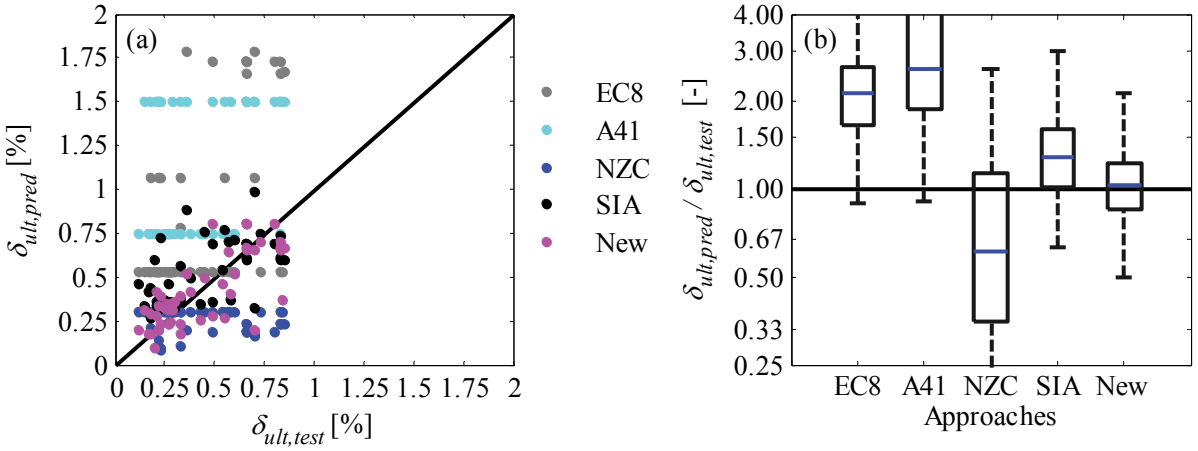

Figure 9. Comparison with code approaches in predicting the ultimate drift capacity of wall tests (only tests with drift capacities smaller than 1 % are considered), (a) predicted vs measured ultimate drift capacity, (b) boxplot

The New Zealand code predictions still remain mostly on the safe side, however, with a large scatter and a low median. Figure 9a illustrates, furthermore, that the proposed approach and slightly less so the SIA formulation appear to capture most trends in drift capacity development as the data points line up in vicinity of the diagonal perfect-fit-line. The EC8, NZC and ASCE 41 provisions seem not to capture

important trends.

5 CONCLUSION

This paper addresses the computation of the effective stiffness and the drift capacity of in-plane loaded URM walls. It analyses a database of URM wall shear-compression tests for trends in stiffness as well as drift capacity. The initial and the effective stiffness appear to depend on the axial load ratio, i.e. the higher the axial load the larger the stiffnesses. Based on the analysis of test results, an empirical formulation for the initial stiffness dependent on the masonry compressive strength and axial load ratio is presented. Furthermore, a G/E ratio of 0.25 is suggested and an effective-to-initial stiffness ratio of 0.75 proposed. As for the drift capacity, the tests indicate that it decreases with increasing normal force and shows an upward trend with increasing shear span, both are relations that have already been indicated by several authors. Furthermore, an existing mechanics-based stand-alone equation for the ultimate drift capacity, evaluating a crushed zone with large curvatures at the wall toe is suggested to be used in engineering practice. Said relation captures the trends indicated by the analyses of the test results. Finally, the proposed formulations for initial and effective stiffness as well as the ultimate drift capacity along with code provisions are compared to a database of 61 full-scale shear-compression tests. It shows that the stiffnesses and the drift capacity are predicted more accurately by the suggested novel formulations than by the considered codes.

6 ACKNOWLEDGEMENT

This study has been supported by the grant no. 159882 of the Swiss National Science Foundation: “A drift capacity model for unreinforced masonry walls failing in shear”.

7 REFERENCES

ASCE, 2014. ASCE 41-13: Seismic Evaluation and Retrofit of Existing Buildings, Reston, VA: American Society of Civil Engineers. Available at: http://ascelibrary.org/doi/book/10.1061/9780784412855.

Benedetti, A. & Steli, E., 2008. Analytical models for shear–displacement curves of unreinforced and FRP reinforced masonry panels. *Construction and Building Materials*, 22(3), pp.175–185. Available at: http://linkinghub.elsevier.com/retrieve/pii/S0950061806002765.

Bosiljkov, V., Tomaževič, M. & Lutman, M., 2004. Optimization of shape of masonry units and technology of construction for earthquake resistant masonry buildings - Part One and Two, *Research Report*, ZAG Lubljana, Slowenia.

Bosiljkov, V., Tomaževič, M. & Lutman, M., 2006. Optimization of shape of masonry units and technology of construction for earthquake resistant masonry buildings - Part Three, *Research Report*, ZAG Lubljana, Slowenia.

Calvi, G.M., 1999. A displacement-based approach for vulnerability evaluation of classes of buildings. *Journal of Earthquake Engineering*, 3(3), pp.411–438.

CEN, 2002. EN 1052-1:1998-12 Methods of test for masonry - Part 1: Determination of compressive strength. European Committee for Standardization, Brussels, Belgium.

CEN, 2005a. EN 1996-1-1:2005 Eurocode 6: Design of masonry structures - Part 1-*1:* General rules for reinforced and unreinforced masonry structures. European Committee for Standardization, Brussels, Belgium.

CEN, 2004. EN 1998-1:2004 Eurocode 8: Design of structures for earthquake resistance - Part 1: General rules, seismic actions and rules for buildings. European Committee for Standardization, Brussels, Belgium.

CEN, 2005b. EN 1998-3:2005 Eurocode 8: Design of structures for earthquake resistance - Part 3: Assessment and retrofitting of buildings. European Committee for Standardization, Brussels, Belgium.

D’Ayala, D.F., 2005. Force and displacement based vulnerability assessment for traditional buildings. *Bulletin of Earthquake Engineering*, 3(3), pp.235–265.

Derakhshan, H., Griffith, M.C. & Ingham, J.M., 2013. Airbag testing of multi-leaf unreinforced masonry walls subjected to one-way bending. *Engineering Structures*, 57, pp.512–522. Available at: http://dx.doi.org/10.1016/j.engstruct.2013.10.006.

Fajfar, P., 2000. A Nonlinear Analysis Method for Performance-Based Seismic Design. *Earthquake Spectra*, 16(3), pp.573–592.

Frumento, S. et al., 2009. Interpretation of experimental shear tests on clay brick masonry walls and evaluation of q-factors for seismic design, *Research Report* EUCENTRE 2009/02, Pavia: IUSS Press.

Ganz, H. & Thürlimann, B., 1984. Versuche an Mauerwerksscheiben unter Normalkraft und Querkraft, *Test Report* Nr. 7502-4, ETH Zürich.

Lagomarsino, S. & Cattari, S., 2015. PERPETUATE guidelines for seismic performance-based assessment of cultural heritage masonry structures. *Bulletin of Earthquake Engineering*, 13(1), pp.13–47.

Lang, K., 2002. Seismic vulnerability of existing buildings. *PhD-Thesis*, ETH Zürich.

Magenes, G., Morandi, P. & Penna, A., 2008. D 7.1c Test results on the behaviour of masonry under static cyclic in plane lateral loads, *Test Report*, ESECMaSE Poject, University of Pavia, EURCENTRE, Italy.

NZSEE, 2016. The Seismic Assessment of Existing Buildings: Technical Guidelines for Engineering Assessments. New Zealand Society for Earthquake Engineering, Wellington, New Zealand.

Ötes, A. & Löring, S., 2006. Zum Tragverhalten von Mauerwerksbauten unter Erdbebenbelastung. *Bautechnik*, 83(2), pp.125–138. Available at: http://doi.wiley.com/10.1002/bate.200610013.

Penna, A., Lagomarsino, S. & Galasco, A., 2014. A nonlinear macroelement model for the seismic analysis of masonry buildings. *Earthquake Engineering & Structural Dynamics*, 43(2), pp.159–179. Available at: http://doi.wiley.com/10.1002/eqe.2335.

Petry, S. & Beyer, K., 2015a. Cyclic Test Data of Six Unreinforced Masonry Walls with Different Boundary Conditions. *Earthquake Spectra*, 31(4), pp.2459–2484. Available at: http://earthquakespectra.org/doi/abs/10.1193/101513EQS269.

Petry, S. & Beyer, K., 2015b. Force-displacement response of in-plane-loaded URM walls with a dominating flexural mode. *Earthquake Engineering & Structural Dynamics*, 44(14), pp.2551–2573. Available at: http://onlinelibrary.wiley.com/doi/10.1002/eqe.2230/full.

Petry, S. & Beyer, K., 2014. Influence of boundary conditions and size effect on the drift capacity of URM walls. *Engineering Structures*, 65, pp.76–88. Available at: http://linkinghub.elsevier.com/retrieve/pii/S0141029614000625.

Priestley, M.J.N., Calvi, G.M. & Kowalsky, M.J., 2007. Displacement-based seismic design of structures, Pavia, Italy: IUSS Press.

Salmanpour, A.H., Mojsilović, N. & Schwartz, J., 2015. Displacement capacity of contemporary unreinforced masonry walls: An experimental study. *Engineering Structures*, 89, pp.1–16. Available at: http://linkinghub.elsevier.com/retrieve/pii/S0141029615000735.

SIA, 2015. SIA 266: Masonry. Swiss Society of Engineers and Architects, Zürich, Switzerland.

SIA, 2014. SIA 269/8: Existing structures - Earthquakes. Swiss Society of Engineers and Architects, Zürich, Switzerland.

SIA, 2011. SIA D 0237: Evaluation de la sécurité parasismique des bâtiments en maçonnerie (Seismic assessment of masonry buildings). Swiss Society of Engineers and Architects, Zürich, Switzerland.

Sterne, J.A.C., 2001. Sifting the evidence---what's wrong with significance tests? Another comment on the role of statistical methods. *BMJ*, 322(7280), pp.226–231. Available at: http://www.bmj.com/cgi/doi/10.1136/bmj.322.7280.226.

TMS, 2008. TMS 402: Building Code Requirements for Masonry Structures. The Masonry Society, Boulder, Colorado.

Tomaževič, M., 2009. Shear resistance of masonry walls and Eurocode 6: shear versus tensile strength of masonry. *Materials and Structures*, 42(7), pp.889–907.

Vanin, F. et al., 2017. Estimates of the stiffness, strength and drift capacity of stone masonry walls based on 123 quasi-static cyclic tests reported in the literature. *Bulletin of Earthquake Engineering*.

Wilding, B.V. & Beyer, K., 2017a. Force–displacement response of in-plane loaded unreinforced brick masonry walls: the Critical Diagonal Crack model. *Bulletin of Earthquake Engineering*, 15(5), pp.2201–2244. Available at: http://link.springer.com/10.1007/s10518-016-0049-7.

Wilding, B.V. & Beyer, K., 2017b. The drift capacity of modern unreinforced masonry walls. *Submitted to Earthquake Engineering & Structural Dynamics*.

Wilding, B.V. & Beyer, K., 2017c. The effective stiffness of modern unreinforced masonry walls. *Submitted to Earthquake Engineering & Structural Dynamics*.